Department of Physics
Astronomy Research Unit

The Ice Particles in Saturn's E Ring and Measurements of the Cassini Cosmic Dust Analyzer and its High Rate Detector

Oskari Tervo

Bachelor's Thesis

2019

Supervisor: Professor Jürgen Schmidt

Contents

1 Abstract

This thesis is a literature review on Saturn's E ring and the respective results obtained by the Cassini Cosmic Dust Analyzer and its subsystem High Rate Detector during Cassini-Huygens mission to Saturn.

The Cassini spacecraft spent 13 years orbiting Saturn while studying the planet, its many satellites and its various rings. One of the most interesting rings to an in-situ instrument is the vast E ring, which originates from the tiny ice-surfaced moon Enceladus. Enceladus' active southern polar region has massive geysir-like phenomena powered by the moon's global subsurface ocean. The jets of (dominantly) water vapor and ice grains are launched to such heights that some of the ice particles do not fall back on the moon and form the E ring. The ring is constantly supplied with new material and it has spread to cover an orbital distance of 1 000 000 kilometers, making it the second largest planetary ring in the Solar System.

The E ring was previously observed with different imaging techniques, but the Cassini opened new research possibilities for in-situ observations with its various instruments. For this thesis, a major focus is the Cosmic Dust Analyzer (CDA) instrument and its subsystem, the High Rate Detector (HRD). The CDA is an instrument for determining properties, such as mass, velocity and mass spectra, of dust particles that collide with it, while the HRD is used to get data on the number of occurring impacts, ie. number density of particles. These properties allowed scientists to determine, for example, the composition of particles within the E ring and the ring's spatial density. The CDA and the HRD had a crucial impact all the way to the last years of the mission where it played a key role in exploring the subsurface conditions of Enceladus and its habitability.

2 The Cosmic Dust Analyzer instrument onboard Cassini

2.1 The Cassini-Huygens mission to Saturn

Cassini-Huygens was a collaboration mission to Saturn by the National Aeronautics and Space Administration (NASA), the European Space Agency (ESA) and the Italian Space Agency (ASI) to Saturn. Its objective was to study the planet, its moons, rings and the planet's magnetic environment. The spacecraft was comprised of two major components: the Cassini orbiter, named after the Italian astronomer Giovanni Domenico Cassini (1625-1712), and the Huygens probe, named after the Dutch astronomer Christiaan Huygens (1629-1695). The spacecraft launched on the 15th of October 1997 and the insertion to Saturn's orbit occured at 1st of July 2004 (ESA 2018). The mission ended on the 15th of September 2017 with a so called "Grand Finale", when Cassini was directed to Saturn's atmosphere where it was destroyed. This end of mission scenario was chosen because it provided a first time opportunity to explore the region closest to the planet and the rings and to prevent a possible contamination of potentially life-sustaining environments with Earthen bacteria or other biomatter.

2.1.1 Huygens probe

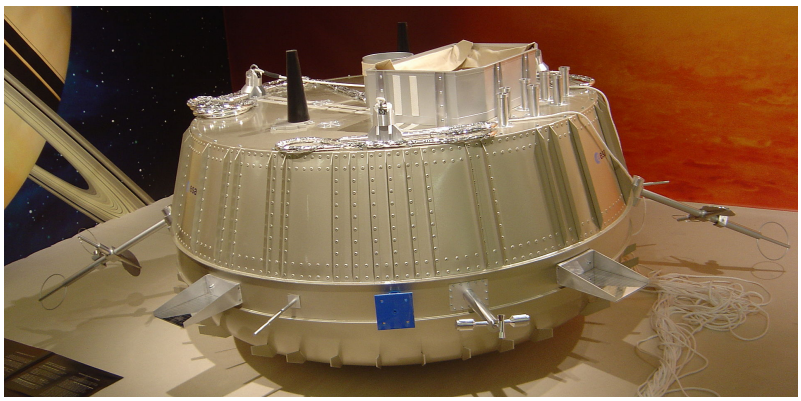

Figure 1: Replica of the Huygens probe (Image: David Monniaux).

This section is based on the online articles "Cassini-Huygens Overview" (ESA 2018) and "Cassini Legacy 1997-2017" (NASA 2018).

Huygens was an atmospheric entry probe manufactured by ESA for the purpose of landing on the surface of Saturn's largest moon, Titan, which was the first attempt to land on a world in the outer Solar System, and at the time of this writing, it is still the only time this feat has been done. The probe was shaped like a small cone, resembling a shellfish (Figure 1) for optimal thermal protection, with a diameter of roughly 2.7 meters and a mass of 318 kilograms. Cassini released Huygens in December of 2004. After 22 days of cruising to Titan and a 2 hour 27 minute descent through Titan's atmosphere, the probe landed successfully on the surface on the 14th of January 2005, where it kept on transmitting signals for 72 minutes. The probe provided unprecedented data about Titan, of which

the most famous are the pictures the probe took during its descent through the atmosphere as well as the ones from the surface of the moon (Figure 2).

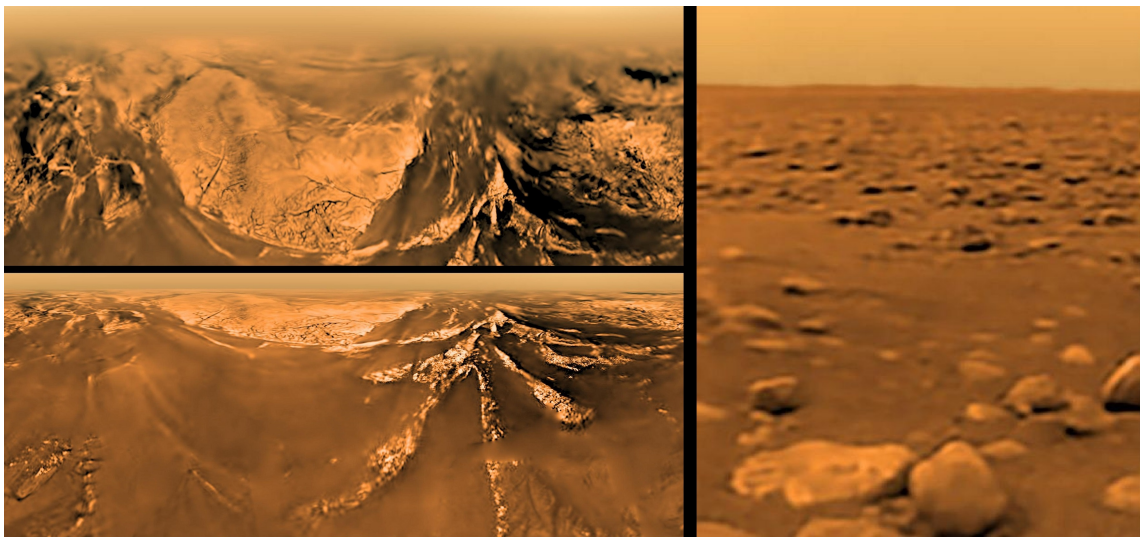

Figure 2: On the left: two pictures taken during Huygens probe's descent to Titan. On the right: a picture taken by Huygens on Titan's surface (Images: NASA).

2.1.2 Cassini orbiter

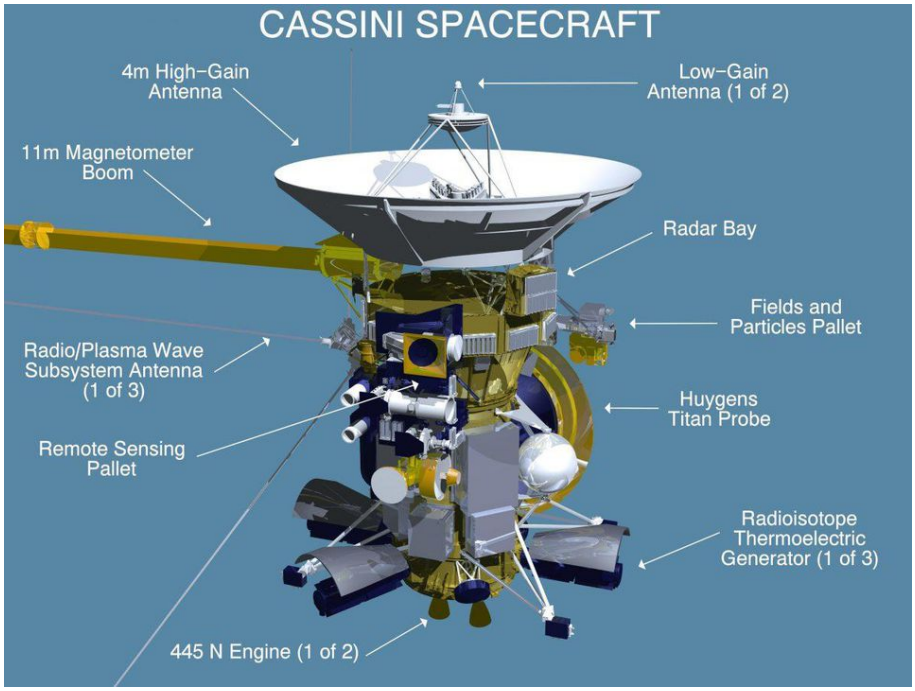

Figure 3: Cassini orbiter and some of its instruments (Image: NASA).

This section is based on an online article "Cassini Legacy 1997-2017" (NASA 2018).

With a weight of 5.6 tonnes, height of 6.7 meters, a width of over 4 meters and equipped with 12 scientific instruments, Cassini (Figure 3) is one of the most ambitious and complex spacecraft created so far. It was manufactured by NASA's Jet

Propulsion Laboratory (JPL). The 12 different instruments, which had been constructed with international contributions and were associated with international science teams, enabled Cassini to perform sophisticated scientific study on various fields: For remote sensing data in the optical range of the electromagnetic spectrum it had the Imaging Science Subsystem (ISS), in the ultraviolet range the Ultraviolet Imaging Spectrograph (UVIS) and in the infrared range the Composite Infrared Spectrometer (CIRS) and Visible and Infrared Mapping Spectrometer (VIMS) components. For microwave remote sensing it had a radar and the Radio Science Subsystem (RSS). To measure particles, fields and waves it had the Cassini Plasma Spectrometer (CAPS), the Ion and Neutral Mass Spectrometer (INMS), the Magnetometer (MAG), the Magnetospheric Imaging Instrument (MIMI), the Radio and Plasma Wave Science (RPWS) and lastly the major focus of this paper, the Cosmic Dust Analyzer (CDA).

The Cassini mission was terminated on the 15th of September 2017 with a controlled entry into Saturn's atmosphere, thus exceeding the originally planned mission end of May 2008 by almost a decade. The collision with Saturn was deemed necessary, because of the slight chance that if Cassini were to be let to orbit Saturn without control indefinitely, it could eventually crash into one of Saturn's moons. Especially for Enceladus and Titan, a contamination of the surface with Earthen bacteria would be a catastrophe to any hypothetical ecosystem on these worlds and the interpretation of results from future missions.

By the end of its mission, Cassini had completed 294 orbits around Saturn with 162 targeted flybys of Saturn's moons. During its lifespan in space of nearly 20 years it collected more than 600 gigabytes of scientific data, making it an invaluably important source of information.

2.2 The Cosmic Dust Analyzer overview

The subsections 2.2, 2.3 and 2.4 are mainly based on the review paper "The Cassini Cosmic Dust Analyzer" (Srama et al. 2004).

The Cosmic Dust Analyzer (CDA) is a versatile tool for dust analysis comprised of two subsystems, the Dust Analyzer (DA) and the High Rate Detector (HRD). Each of these subsystems has subcomponents of its own for specific tasks, which will be looked at in more detail in the following subsections.

The CDA can infer with its subsystems the properties of dust particles based on the data received when dust particles collide with the instruments. Because collisions are the basis for all the data, it is vital that the CDA can be orientated such that it can detect the most amount of impacts during all times. In addition to the possibility of changing the spacecraft orientation, this is achieved with a turntable (Figure 4), which allows adjustment of the pointing of the CDA instrument axis to optimize particle flux for a given geometry. Realistically, however, the instrument is not always pointed optimally, because measurements of other instruments may define how Cassini itself is orientated, which naturally affects the pointing of the CDA. Major limitation is that the sensors' geometric detection probability is drastically decreased when particles are colliding with a large an-

gle from the instrument axis. For example, the Chemical Analyzer of the Dust Analyzer can not detect particles with an incidence angle of greater than 28°.

2.3 The Dust Analyzer subsystem

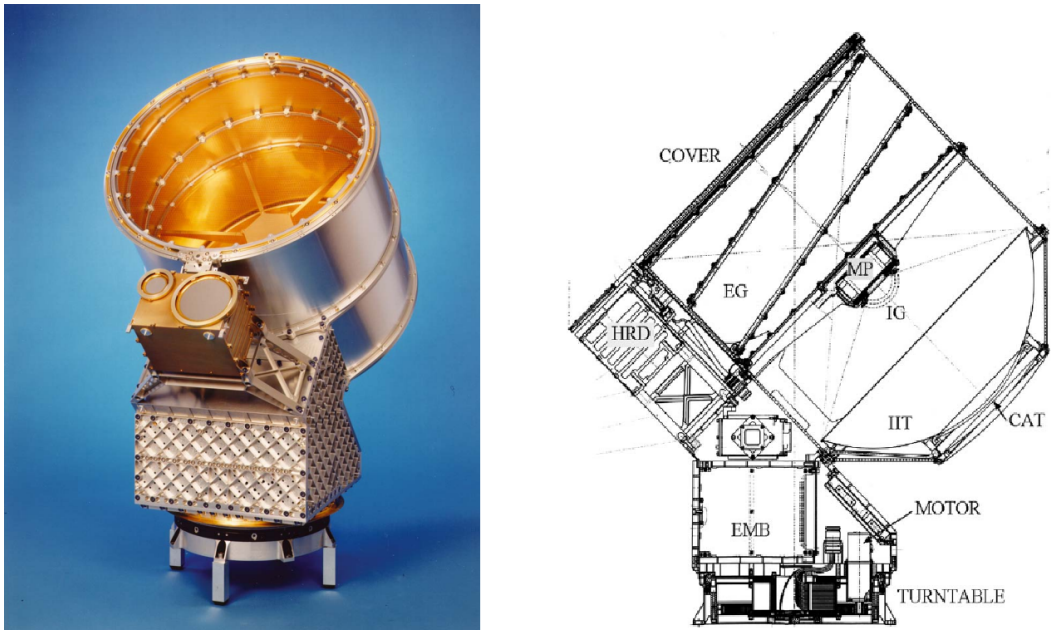

Figure 4: On the left: Cassini's Cosmic Dust Analyzer. The big "drum" is the DA instrument and the box with two plates is the HRD instrument. On the right: schematic view of the CDA with its subsystems (Figure reproduced from Srama et al. 2004, Space Science Reviews, vol. 114, p. 465-518, Figures 1 & 2).

While being itself a subsystem of the CDA, the Dust Analyzer (DA) is also comprised of its own subsystems: the charge detector (entrance grids, EG), the Impact Ionization Detector (IID) and the Chemical Analyzer (CA).

The charge detector is a system of two stainless steel grids located at the front end of the DA. When a charged particle enters the DA, it will induce a charge in the grids, which has a direct correspondence to the charge of the particle. The system has detected particle charges as low as $Q = 10^{-15}$ C. For a typical electric potential of $V_E = -5$ V, this charge would correspond[1] to a particle with a radius of $\approx 1.80 \times 10^{-5}$ m. The two grids are positioned on the edges of the DA (Figure 4, EG) and when a particle goes through them, each of the grids detects its charge. The duration of these charge detection signals can be used to determine the particle's velocity. The velocity obtained is used for verification and calibration of indirect determination of particle speed based on signals from impact ionizations.

Particle composition analysis is resulted from impacts with Chemical Analyzer Target (CAT) or Impact Ionization Target (IIT): When particles collide with either target, they produce particle and target fragments, neutral atoms, ions and electrons of which data is collected and analysed by the Chemical Analyzer. The

[1]Electric potential formula $V_E = \frac{1}{4\pi\varepsilon_0}\frac{Q}{r}$, where ε_0 is the permittivity of vacuum (Horányi 1996).

sensors of these subsystems cover a large dynamic range: they are by design able to detect properties of particles with a mass range of six orders of magnitude. Impacts are classified as events, which will immediately be analyzed whether their quality is good, poor or if they are simply noise. An integer counter in the datafiles is increased for each event and with it information like time when the event occurred, the impact location etc. are written. A major thing of note with the DA datafiles is that when an event occurs, the instrument is insensitive for about 1 second to allow time to process the complex data, which results the data events in the files being spaced by one second at least. In very dense dust environment this instrumental dead time hampers, or makes impossible, the measurement of the particle density. To obtain reliable counts of grains in such dense environments, the CDA has the HRD subsystem.

2.4 The High Rate Detector subsystem

2.4.1 Overview

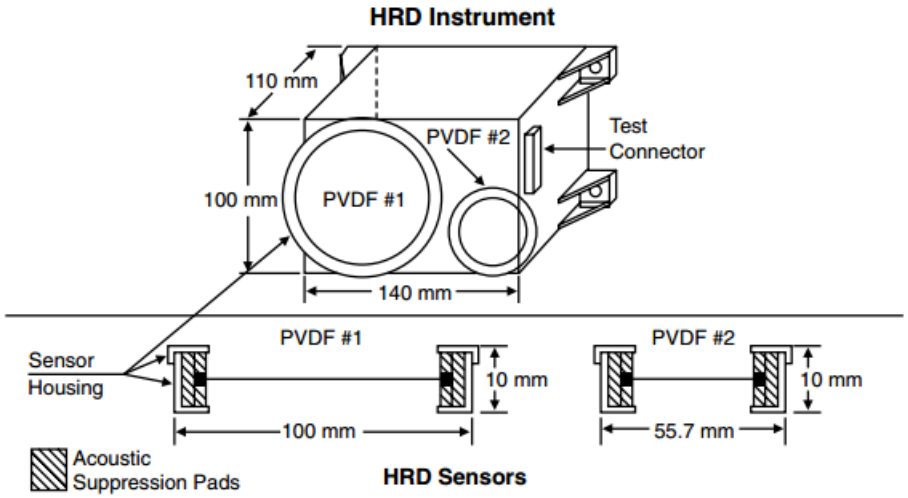

Figure 5: Detailed view of the HRD and its sensors (Figure reproduced from Srama et al. 2004, Space Science Reviews, vol. 114, p. 465-518, Figure 10).

The High Rate Detector is a subsystem built by Anthony Tuzzolini (1931-2008) (University of Chicago News 2008) at the University of Chicago, meant to measure particle flux and particle mass distribution. Its design is heavily based on similar instruments (also by the team from University of Chicago) used earlier on spacecraft Vega-1 and Vega-2, which observed Halley's Comet (Srama et al. 2004). Shaped like a rectangular box (dimensions 100 mm x 140 mm x 110 mm), it has two circular detector plates with different areas (Figure 4). The HRD is able to detect particle impacts up to a rate of 10^4 impacts per second. Because it is rigidly attached to the DA, the HRD's pointing can be adjusted with the orientation of the CDA. In cumulative flux measurements it can detect particles with a mass greater than 8×10^{-13} grams. This limiting mass is defined for an assumed particle velocity of 15 km/s. Even though the HRD's pointing is dependent on the CDA as a whole, the HRD is an independent instrument with its own memory

and processor.

2.4.2 Detector counters

The detector counters' sensors are of polyvinylidene fluoride (PVDF), which is spread as a thin foil between acoustic suppression pads (Figure 5). The larger counter, PVDF #1, has a diameter of 100 mm, an area of 50 cm^2 and a 28 μm foil thickness. For the smaller counter, PVDF #2, the same respective values are 55.7 mm, 10 cm^2 and 6 μm. Both foils are of permanently polarized material and when a particle collides with them, it causes a depolarization which can be detected as a brief current — a pulse. The resulting pulses are fast enough to enable the high detection rate of 10^4 impacts per second. Such high detection rates are of great importance during ring plane crossings in the region of the E ring and other dust rings in the system as well as and crossings of the Enceladus plume.

Each of the plates has four different mass thresholds (each with their own counters in the datafiles) for identifying particles of different sizes. For PVDF #1 they are labelled in the datafiles as M1, M2, M3 and M4 and for PVDF #2 m1, m2, m3 and m4 from smaller to larger threshold for both sensors. The mass thresholds can also be understood as charge thresholds. These charges are produced by the number of electrons n resulting from an impact with the detector and this value is dependant on the dust particle mass m_d and velocity v_d as

$$n_M = 3.8 \cdot 10^{17} (m_d[kg])^{1.3} (v_d[km/s])^{3.0}$$

for the M-sensors (PVDF #1) and

$$n_m = 3.6 \cdot 10^{18} (m_d[kg])^{1.3} (v_d[km/s])^{3.0}$$

for the m-sensors (PVDF #2) (Kempf et al. 2012 equations 1.8 and 1.9). The mass threshold values for ice particles[2] with a velocity of 15 km/s and a typical density of $\rho = 0.9$ g/cm^3 can be found in Table 1. Similar to the DA, the data products of the HRD are also updated at every second at maximum, which is disadvantageous during high activity periods.

Due to the sensitivity of the foils, manoeuvres of the spacecraft's jet engines, the reaction wheels, moving platforms and the like could potentially trigger the PVDF foils to give false events that have nothing to do with particle impacts. To lessen the likelihood of this happening, the sensors are mounted on sound absorbing pads. The sensors are also coated with Chemglas Z-306 (Kempf et al. 2012) for thermal protection, because they are sensitive enough that a temperature of 80 °C would damage them permanently. While a temperature this high could not occur while in the Saturnian system, it could have occured in the inner Solar System during the cruise phase of the mission.

[2]Mass thresholds are calculated from the equation $m = \rho \frac{4}{3} \pi \left(\frac{d}{2} \right)^3$, where particles are assumed spherical and their diameter d is expected not to change from Srama et al. 2004 Table XI.

Threshold	Lower limit (g)	Upper Limit (g)	Particle Diameter Range (μm)
M1	1.6×10^{-12}	7.4×10^{-12}	1.5 - 2.5
M2	8.3×10^{-12}	6.1×10^{-10}	2.6 - 10.9
M3	1.8×10^{-9}	2.0×10^{-8}	15.7 - 35
M4	3.0×10^{-8}	3.3×10^{-7}	40 - 89
m1	2.4×10^{-13}	2.1×10^{-11}	0.8 - 1.5
m2	1.6×10^{-12}	1.7×10^{-9}	1.5 - 8.8
m3	8.3×10^{-10}	5.5×10^{-8}	12.1 - 36.7
m4	3.1×10^{-8}	9.3×10^{-7}	40.2 - 124

Table 1: Mass limits of sensor thresholds and the corresponding particle diameter ranges for ice particles with a density of $\rho = 0.9$ g/cm^3 and velocity of 15 km/s. Particle diameters are from Srama et al. 2004 Table XI. Maximum error for the masses is 10% (Schmidt et al. 2017).

Overall, The HRD was expected to experience temperatures between -50 to 80 °C (Srama et al. 2004). The variation of temperature would affect the sensor capacitance and also the depolarization of the foils during particle impacts. The combined effect of these two phenomena on the depolarization currents was estimated to be 10% at maximum over the entire expected temperature range (Srama et al. 2004). This results in an insignificant error in the particle mass thresholds.

An important note is that one of HRD's sensor plates was slightly damaged during a G ring passage in 2006 making of of the mass thresholds noisy. Luckily, the instrument remained operational, but this meant that the quality of HRD data was lessened for the rest of the mission (Horanyi et al. 2009).

3 HRD measurements in the Saturnian system

3.1 Enceladus plume

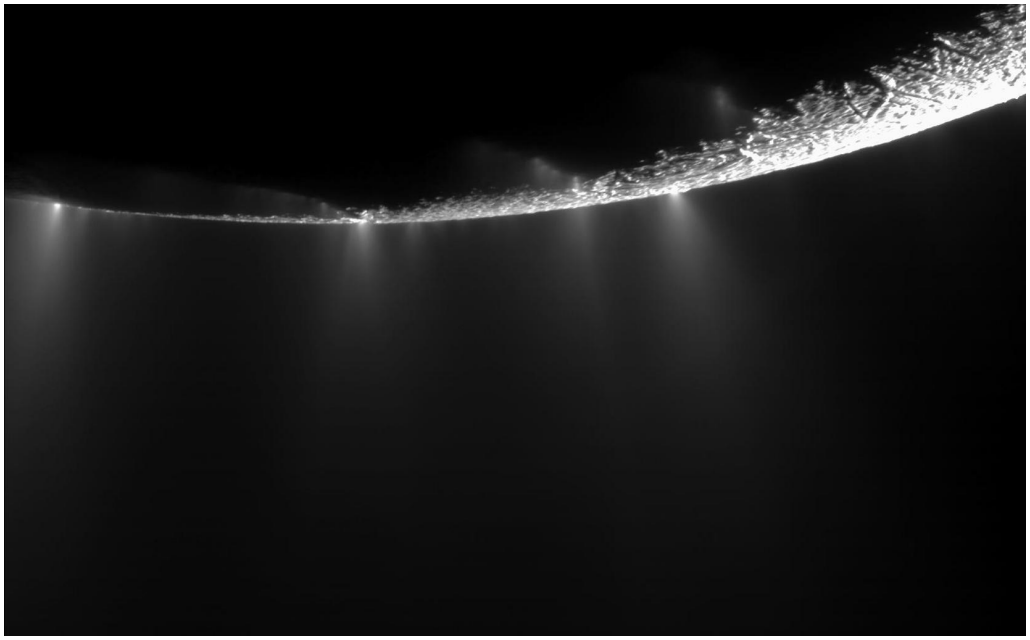

Figure 6: Enceladus' south polar region and its plumes (Image: NASA).

Discovered in 1789 by William Herschel, Enceladus is Saturn's sixth largest moon with a mean radius of 252.1 km. It has a semi-major axis of 328 037 km and a low eccentricity of 0.0047. Its surface is entirely covered with fresh, clean ice, which makes it the most reflective object in the Solar System. Beneath the icy surface with a thickness of approximately 26-31 km lies a global subsurface ocean, according to current knowledge (Thomas et al. 2016).

The moon has a highly active south polar region where the "tiger stripes" lie. These stripes are four large fractures surrounded by ridges. The stripes were revealed to have higher temperature than the rest of the moon's surface by thermal imaging (Spencer et al. 2006; Howett et al. 2011). Cassini found in 2005 that the stripes are the origin of the now-iconic Enceladus plume (Spahn et al. 2006; Porco et al. 2006) — a geysir-like phenomenon where vapor from the subsurface ocean erupts from the stripes' fissures in a process similar to an erupting volcano, hence the name cryovolcanism. The water heated by Enceladus' rocky core (Choblet et al. 2017) makes the ice shell thinner at the south pole. Cracks in the thinner ice allow water to seep ever closer to the surface.

To keep the liquid water ocean from freezing, Enceladus' core must produce or receive heat. However, Enceladus is so small in size that it does not have a molten core, so it must get its heat through other means. Choblet et al. 2017 suggest heating from radioactive decay and strong tidal heating that is enhanced by the porosity of Enceladus' core.

The majority of the water particles ejected by the plumes fall back on the surface and cover it, which explains the low amount of craters on Enceladus.

However, Enceladus' gravity is weak and some of the particles manage to escape from Enceladus' gravitational influence. These particles form the vast E ring.

3.2 E ring

3.2.1 Overview

This section is mainly based on the chapter 16.3.8 of the book "Saturn from Cassini-Huygens" (Horanyi et al. 2009).

Figure 7: Saturn's rings and the locations major moons' orbits in relation to them (Image: NASA).

The E ring is the second-most expansive planetary ring in the Solar System (after the Phoebe ring, Section 3.4.1), spanning an orbital range of more than 1 000 000 kilometers between the orbits of the moons Mimas (semi-major axis 185 000 km) and Titan (semi-major axis 1 221 000 km). In total, it envelops 6 satellites, which are with increasing distance from the planet Mimas, Enceladus, Tethys, Dione, Rhea and Titan (Figure 7). In addition to its size, the E ring differs from the main rings of Saturn because it is comprised of microscopic particles (scale of $\sim \mu$m) instead of macroscopic (scale of a few centimeters to tens of meters). As mentioned in Section 3.1, the source of particles are Encaladus' plumes. Approximately 5-50 kilograms worth of plume particles are produced every second (Schmidt et al. 2008; Ingersoll and Ewald 2011). Particles with a radius of 1 μm are estimated to have a mean velocity of 120 m/s (Horanyi et al. 2009) and about 1% escape Enceladus and are thus added to the E ring. The ring's thickness increases linearly from its densest point (Kempf et al. 2008), which is roughly 3000 km outward from Enceladus' orbit. Dikarev 1999 and Juhász et al. 2007 have shown that the densest point is displaced from Enceladus' orbit due to plasma drag.

Walter Feibelman (1925-2004) was the first to discover E ring's existence in 1967, but this was not confirmed until 1979 by the Pioneer 11 spacecraft flyby (Oergerle 2004). After its discovery, the ring has been investigated with ground- and space-based imagery (Horanyi et al. 2009). When Cassini inserted on Saturn's orbit in 2004, new opportunities for the scientific investigation of the E ring

were enabled with the instruments onboard. Flybys through the E ring and the resulting particle detections with the CDA gave vast quantities of information which was unavailable before this.

3.2.2 Particle properties

This section is mainly based on the article "The E-ring in the vicinity of Enceladus II. Probing the moon's interior — The composition of E-ring particles" (Postberg et al. 2008).

Thanks to the CDA, the E ring particles' chemical composition could be analyzed for the first time. It was found that the majority of particles are water ice. Three spectral types were identified: Type I of almost pure ice and small amounts of sodium. Type II had impurities of organic compounds and/or silicate minerals with the ice. Postberg et al. 2009 suggest that a small part of Type I particles might be ejecta launched to space from micro-meteoroid impacts with Enceladus' surface and Type II are thought to originate exclusively from Enceladus' ice geysirs. These two types are found everywhere in E ring, which tells that the particles disperse quickly throughout the ring. There also exist a more minor particle population, Type III, which has sodium-rich water ice ($\sim 0.5 - 2\%$ of the mass is sodium salts) (Postberg et al. 2009).

For particles with a size larger than 0.9 μm, the radial distribution can be described fairly well with a pair of power laws centered at and decreasing with distance from the densest point of the ring. As mentioned in Section 3.2, the densest point is distanced roughly 3000 km outwards from Enceladus' orbit. From there, the density decreases roughly in accordance with the power law with distance from Enceladus. However, the vertical thickness increases linearly with distance from the densest point (Section 3.2). Highest measured number densities thus far have been from 0.16 to 0.21 per m^3 for particles larger than 0.9 μm and from 0.021 to 0.076 per m^3 for particles larger than 1.6 μm (Horanyi et al. 2009).

Earliest measurements of E ring particles' charge are by the Voyager spacecraft, which determined that inside 6.5 R_S (R_S = Saturn's radius = 58 232 km) all particles had a negative charge, while beyond 7.5 R_S the charge was positive. Cassini later improved on these results when it found that the orbit of the moon Rhea is roughly the boundary between the charges of different sign (Kempf et al. 2006). It is in this region where the direct currents from the ambient plasma are less important and photoelectron emission becomes relevant, resulting in a positive grain charge. Particles were also found to have a potential ranging from -2 to -3 V between distances of 2.5 to 5 R_S.

3.3 G ring

This section is mainly based on the article "The Source of Saturn's G ring" (Hedman et al. 2007).

The G ring is one of the outer rings of Saturn located near the orbit of the moon

Mimas at approximately between 165 000 to 175 000 km from Saturn's center (Figure 7). The precise boundaries are difficult to define as even though the G ring has a sharp inner edge, the outer boundary gradually blends into the background E ring (Horanyi et al. 2009). The majority of G ring's particles are on a scale of μm, similar to E ring.

The most prominent feature of G ring is a bright arc on the ring's inner edge, which spans one sixth of the ring's circumference (longitude of ~60°) and has radial full width at half maximum (FWHM) of roughly 250 km. The arc's orbital mean motion is estimated to be 445.475° ± 0.007° / day and this corresponds to a semi-major axis of 167 495.6 ± 1.3 km (Hedman et al. 2007). Cassini's observations have revealed the arc to be a permanent feature of the G ring. The material forming the arc is in a 7:6 corotation resonance with Mimas and it is known to consist of centimeter to meter-sized particles. Measurements have shown that their total mass is equivalent to that of a ~100 meter wide ice-rich moonlet.

Before Cassini's arrival, there was no obvious explanation for G ring's location, because there were not any known nearby sources which could replenish the dust in the ring (the orbit of the nearest satellite Mimas is 15 000 km away). Now it is known that G ring's dust originates from within the bright arc, from where the dust drifts out into the main ring due to interaction with Saturn's magnetosphere. In 2009, the tiny, elongated satellite Aegaeon (Green 2009) (dimensions of only $\sim 1.4 \times 0.5 \times 0.4$ km) was discovered within the G ring's arc and it too is in a 7:6 corotation resonance with Mimas. Aegaeon is thought to be one of the sources of dust inside the arc, but not the only one (Madeira et al. 2018).

3.4 Other dust complexes in the Saturnian system

3.4.1 Phoebe ring

The Phoebe ring was discovered in 2009 with NASA's Spitzer Space Telescope (Verbiscer et al. 2009) and it is by far the vastest ring in the Solar System (Figure 8). At first, it was thought to span an orbital range between 7.7 to 12.4 million kilometers from Saturn (~128 to ~207 Saturn's radius $R_S \approx 58\,232$ km), but more recently it has been shown to stretch from orbital range of 6 million km to 16.2 million km (~100 to ~270 R_S) (Choi 2015). Even though the ring is very large, it is not dense: one cubic kilometer of space within Phoebe ring is suspected to contain at most only 100 particles (Choi 2015).

The ring gets its name from the largest outer Saturnian moon, Phoebe, which is suspected to be the main source of the ring. Phoebe is located within the ring with a semi-major axis of 12.96 million kilometers and while yet unclear, Hamilton et al. 2015 suggest it supplies the ring with particles ejected from the moon. They also suggest that other smaller Phoebe-like satellites[3] could be a potential source, possible even more important than Phoebe itself. The particles themselves are mostly ranging from 10 to 20 μm in size and size distributions show that rocks with a diameter of 20 centimeters or more make up only 10% of the

[3]With similar orbital inclinations: Phoebe is retrograde, with an inclination of 175° relative to the ecliptic plane.

ring particles, at most (Choi 2015; Hamilton et al. 2015). Because of the ring's size and the small number of large satellites within it, the Phoebe ring particles are millions, possible even billions of years old, as they have a very low chance of collision with other bodies in the system, unlike the main ring and E ring particles (Choi 2015).

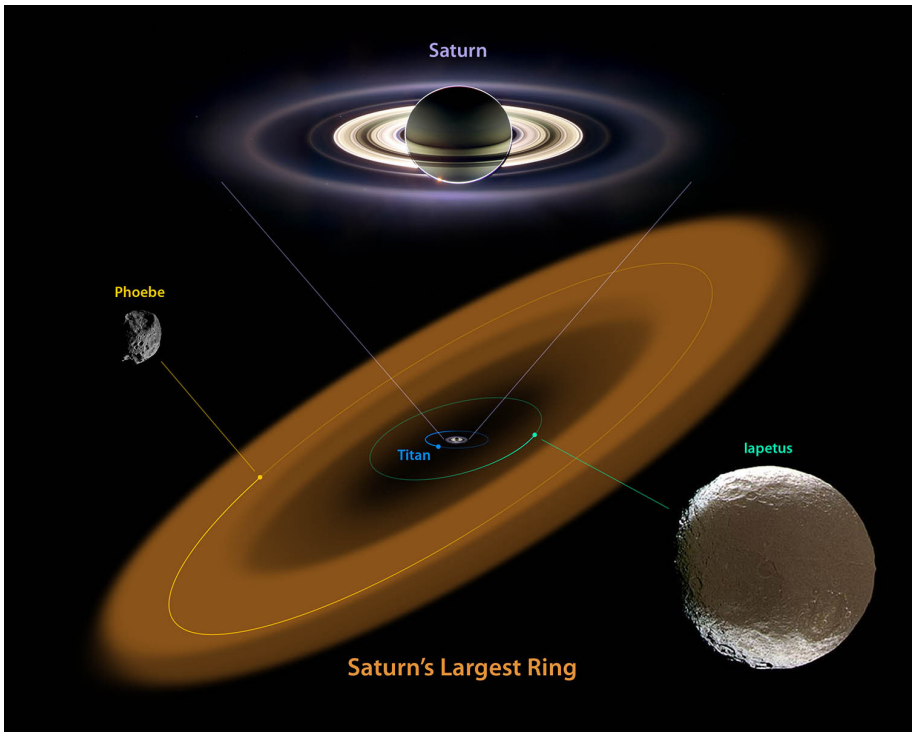

Figure 8: Phoebe ring and its size relation to Iapetus' and Phoebe's orbits. Note the orbit of Titan, inside of which is the E ring — the second largest ring (Image: NASA).

3.4.2 Iapetus

This section is mostly based on the online article "Iapetus, in depth" (NASA 2017a).

Discoved by Giovanni Cassini (Section 2.1) in 1671, Iapetus is the third largest satellite of Saturn. With a semi-major axis of ~ 3.56 million kilometers, it orbits relatively close to the inner border of the Phoebe ring (Figure 8). The moon's surface has striking surface features in that its opposite faces are of opposite colors (Figure 9) and the cause for this was first suspected to be collision with ring particles (Choi 2015). At the time of this writing, the most probable explanation for this is different: because of the tidal locking with Saturn, Iapetus rotates around its axis once in every 79 (Earthen) days and with this, it has the longest day-night cycle of all the major satellites in the Saturnian system. During daytime, the long exposure to the sunlight on the darker region, which absorbs more heat, will cause icy material to sublimate and retreat to the colder side of the moon. This in turn makes the dark material even darker (and more absorbent), which would accelerate the sublimation process (Spencer and Denk 2010).

Other major features of the moon include large impact craters (Figure 9) and the Voyager mountains, which is a 10 km high nearly circumferential mountain

range on the equator of the moon. Because the moon has a mean radius of only ~ 735 km, the mountains are a very striking feature and can be seen protruding out against the background of empty space in Figure 9.

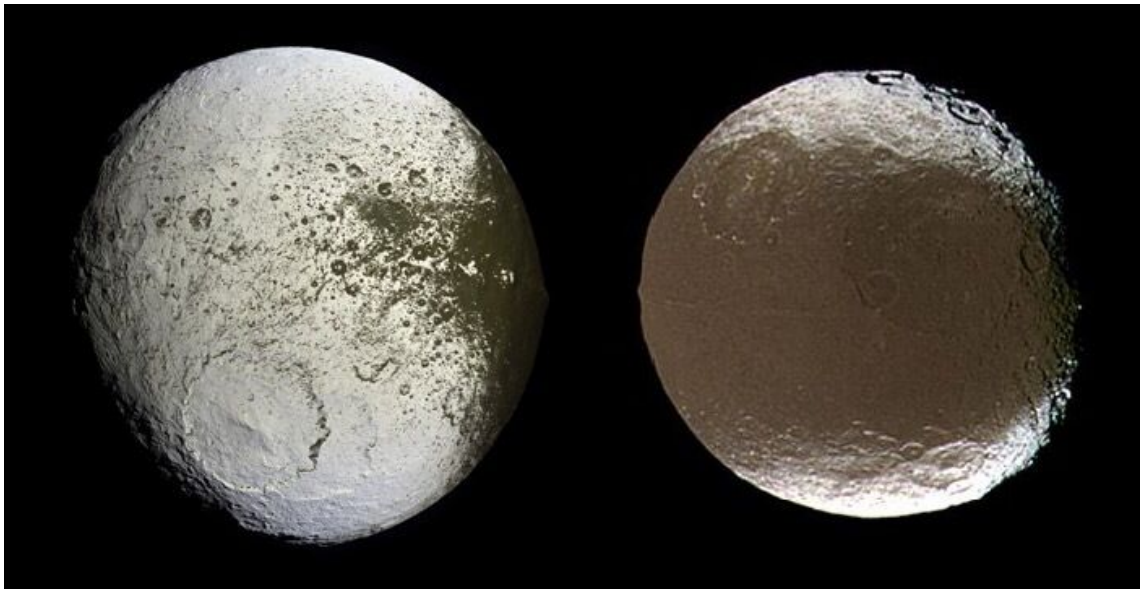

Figure 9: The moon Iapetus and its opposite faces. The dark side is always pointing towards the direction of orbital motion (Image: NASA).

3.4.3 Dust rings in the main rings

The D ring is Saturn's innermost ring, from roughly 67 580 to 73 145 kilometers from Saturn's center ($R_S \approx 58\ 232$ km). Because of its vicinity to the planet and small particle sizes (from 1 to 100 μm), it is very challenging to image from Earth. The D ring contains 3 major ringlets, for which changes in brightness and position have been observed over the last few decades (Hedman et al. 2006).

R/2006 S3, nicknamed "Charming ringlet", is found in the Laplace gap of the Cassini division, some 119 940 kilometers from Saturn's center. The ringlet has a peculiar property, where its geometric center is more distant from Saturn's center near sub-solar longitudes than on longitudes in proximity of Saturn's shadow. This suggests that the ringlet's dynamics are affected by the solar radiation (Hedman et al. 2010).

Sun et al. 2015 studied the central ringlet in the Encke gap (133 581 km from Saturn's center), which is mainly comprised of micron-sized particles. The moon Pan orbits within the Encke gap and it was concluded that it cannot sustain the central ringlet with enough dust on its own. Possible undetected moonlets were also considered as a potential source, but they were found to simultaneously be dust sinks as well as sources.

3.4.4 Pallene dust

Discovered by the Cassini spacecraft in 2004, Pallene is a tiny moon (~ 2.5 km mean radius) orbiting Saturn with a semi-major axis of roughly 212 000 km, placing it close to the inner boundary of the E ring. Together with the moons Methone

(mean radius of $\sim$ 1.5 km) and Anthe (mean radius of $\sim$ 1 km), it belongs to a group called Alkyonides, which can all be found between the orbits of Mimas and Enceladus (NASA 2017c). Measurements by the CDA showed the dust particles to be around 1 μm in size and that the ring's maximum particle density is $2.7{\times}10^{-3}$ particles per m^3 (Seiss et al. 2014).

Pallene has a ring along its orbit (Hedman et al. 2009), the Pallene ring, which highly suggests that the moon is the ring's source, possibly due to meteoroid impacts with the moon's surface (NASA 2017c). The ring has a radial extent of about 2 500 km and is very faint, which make observations challenging. The other Alkyonidean moons have dust-related structures with them as well, but unlike the Pallene ring, these features are more akin to arcs, instead of continuous rings (Hedman et al. 2009). It is suspected, that the Alkyonidean moons may also be a source of particles for the E ring (NASA 2017c).

4 Main results from CDA and HRD

4.1 Enceladus Subsurface ocean and the hydrothermal vents hypothesis

One important indication for the existence of a subsurface ocean on Enceladus was the discovery of particles with high concentration of sodium (spectral Type III, Section 3.2.2) within the Enceladus plume (Postberg et al. 2009). Because sodium is considered a tell-tale sign for a reservoir of liquid water and the long periods of activity of individual plumes, it was deemed that there is an ocean below Enceladus' surface. This was confirmed by Cassini measurements of the libration Enceladus has while orbiting Saturn, which indicates that the moon's core is not solidly attached to the surface (Iess et al. 2014; Thomas et al. 2016).

During Cassini's last flyby of Enceladus in 2015, the spacecraft discovered molecular hydrogen (H_2) in the plume (Waite et al. 2017). The origin of the H_2 was puzzling, because it is too volatile that it could be found among the active ice surface as pre-existing reservoir (or that it had originated from somewhere other than on Enceladus), so it had to be produced below the ice. Enceladus' ocean does not have enough H_2 to sustain the amount detected in the plume, so an origin in hydrothermal vents in the moon's rocky core was suggested as a source (Waite et al. 2017).

Hydrothermal vents are well known from the Earth: on our planet, they are fissures on the ocean floor, where geothermally heated water meets the ocean and are commonly located near volcanically active regions. The hydrothermal reactions between rock and water can produce large amounts of H_2 on Earth and this is likely for Enceladus too, as many other alternatives were deemed not significant enough in relation to the amount of H_2 observed (Waite et al. 2017). Earlier observations of SiO_2 (silica) nanoparticles by the Cassini CDA (Hsu et al. 2015) first suggested this hydrothermal vent hypothesis, as the detected particles are a sign of hydrothermal activity, because their formation requires ongoing high-temperature (at least 90 °C) producing processes (Hsu et al. 2015).

In our oceans, hydrothermal vents typically have rich ecosystems around them. What makes them very special, is that they are the only known ecosystems which are entirely independent of the Sun as a source of energy. It is known that life on Earth originated from oceans and hydrothermal vents are currently believed to be the most likely source where earliest lifeforms developed. Life as we understand it requires liquid water, an energy source for the metabolism and essential elements, like carbon, oxygen and sulfur, and these conditions are met at the hydrothermal vents on Earth. The vents on Enceladus could also fulfill these criteria, which makes the moon a highly important candidate in the search for biological life outside Earth (NASA 2017b).

Hydrothermal vents are possible on Earth because of the tectonic plates' activity and the molten core of the planet. On Enceladus, however, the core is not molten (Section 3.1) so the existence of these vents is closely connected to the question of what keep Enceladus' ocean from freezing, ie. where does it get its heat from.

4.2 Enceladus' south pole as the origin of the E ring and Enceladus plume particle profiles

When the origin of the E ring was still in question, one of the possibilities for the source of the ring's particles was thought to be micrometeoroid impacts on Enceladus' surface. As Enceladus is very close to the densest point of the E ring (Section 3.2), scientist suspected the icy moon to be the ring's source. Based on the Cassini High Rate Detector data obtained during the Enceladus flyby on 14th of July 2005, Spahn et al. 2006 modelled a profile for plume particles (Figure 10). In the figure, the peak detection rate is observed roughly 1 minute before the closest approach, which was a very important fact: The team had created computational models for micrometeoroid impacts with the moon calculated the corresponding dust distribution.

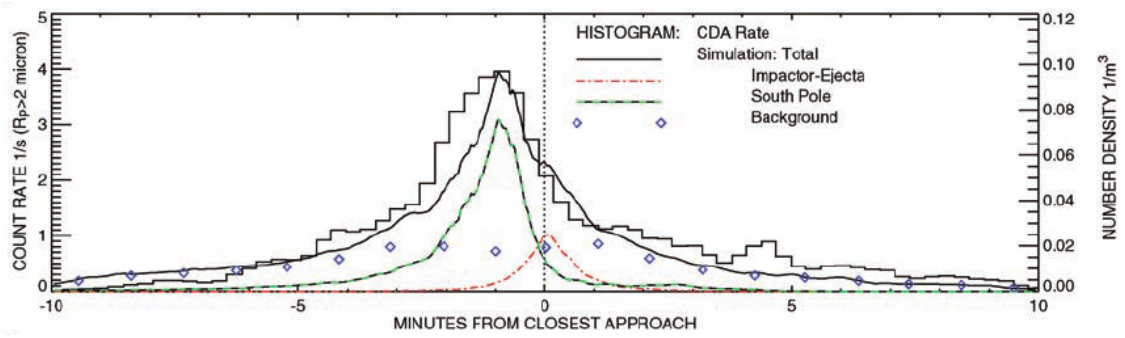

Figure 10: HRD particle count rates from the 50 cm^2 detector plate as a function of minutes from the time of closest approach. A later, refined, calibration of the detector showed that the instrument was sensitive to grains larger than 1.6 μm on this flyby, not 2.0 μm as originally believed (Postberg et al. 2011). The peak detection rate is slightly displaced from the point where Cassini was closest to Enceladus, which was an important factor in determining the origin of the particles (Figure reproduced from Spahn et al. 2006, Science, vol. 311, p. 1416-1418, Figure 1B).

The models showed that in this case the dust would spread uniformly around the moon and the resulting the peak detection rate would always be observed at the point of closest approach during flybys. Since these models did not match the observations, the micrometeoroid theory was abandoned. At the time, the unusually high temperature of Enceladus' south pole was known (Spencer et al. 2006), so the team focused on simulations where the source of the particles was placed in and around the polar region. Spahn et al. 2006 created simulations where the origin of the particles was systematically changed around the south pole and corresponding (theoretical) particle densities were calculated along the flightpath of the Cassini. It was found that the best match was when the origin was placed within the "tiger tripes" (Section 3.1), which reproduced a delay of 1 minute from the closest approach matching the observations. The team concluded the south pole's tiger stripes as the origin of the particles, which was later confirmed (Section 3.1).

4.3 The spatial distribution of the E ring particles

This section is based on the article "The E ring in the vicinity of Enceladus I. Spatial distribution and properties of the ring particles" (Kempf et al. 2008)

Kempf et al. 2008 were focused on determining the vertical and radial ring profiles of the E ring with data obtained during multiple ring plane crossings between years 2005 and 2006. The data used was solely from the HRD as the Dust Analyzer subsystem of the CDA is saturated when the spacecraft is within the E ring inside about 5 R_S. The best results for vertical ring profiles are obtained when the angle γ_X at which the spacecraft pierces the ring plane is large: the larger γ_X is, the lower is the dependence of the observed impact rates on radial variations of the density.

The plotted vertical density data (Figure 11) suggests that the densest point of the E ring is displaced outward from Enceladus' orbit by at least 0.05 R_S. It was also found that for particles with a size >1 μm, the ring profile is highly Gaussian and the Full Width at Half-Maximum (FWHM) is ~ 4300 km at Enceladus' orbit. At Mimas' orbit FWHM increases to ~ 5400 km. However, outside of Enceladus' orbit, the profile does no longer resemble a Gaussian.

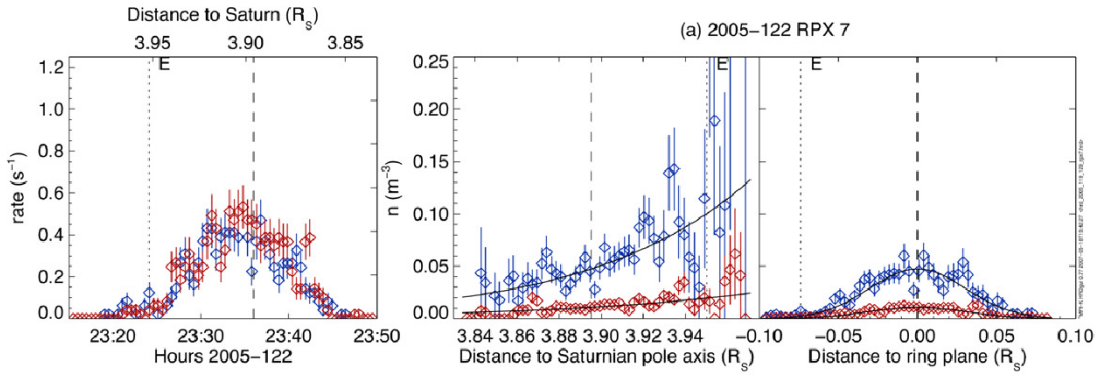

Figure 11: From left to right: Impact rate as a function of time, distance to Saturn and distance to the ring plane. The plots are based on data obtained during ring plane crossing on 2nd of May 2005. The dotted vertical line is Enceladus' orbit and the broken line where Cassini crossed the ring plane (Figure reproduced from Kempf et al. 2008, Icarus 193, p. 420-437, first dataset of Figure 3).

5 Summary

The substantial amount of in-situ data obtained by the Cassini DA and the HRD have led to a number of new discoveries and innovations:

E ring was found to be more massive than originally thought, stretching all the way to Titan's orbit. Through HRD measurements, we have a better understanding of the ring's radial and vertical profiles. A plume was discovered and later directly detected on the southern pole of Enceladus and eventually confirmed the moon as the source of the E ring. Data gathered from the plume and the E ring revealed information about the composition of Enceladus' interior. This data led to the conclusion that there is water and organic material below the moon's icy surface and their respective origins being a subsurface ocean and hydrothermal activity. Even though Cassini's mission ended in September of 2017, new discoveries are still being made. More recent results include observations of complex organic molecules (Postberg et al. 2018), unprecedented data about the proximal orbits of Saturn (Hsu et al. 2018), measurements of Saturn's interior's rotation period (Mankovich et al. 2019) and estimates on the age and mass of Saturn's rings (Iess et al. 2019).

Future prospects include a return to the Saturnian system and concept studies have already begun in the US and Europe. Now that we have a better understanding of what to except in the system, measurements would be much more accurate with specifically tailored instruments of newest technology. Enceladus and its plume could be observed far better, as the CDA was not designed for such purpose: organics and plume particles could be identified more clearly and potential products of biological processes discovered. Possibilities of a lander or a sample return from the system have also been discussed. In whatever manner the mission will end up being realised, it will no doubt be a worthwhile endeavour.

6 References

Choblet, G., G. Tobie, C. Sotin, M. Běhounková, O. Čadek, F. Postberg, and O. Souček (2017). "Powering prolonged hydrothermal activity inside Enceladus". In: *Nature Astronomy, vol. 1*, pp. 841–847.

Choi, Charles Q. (2015). *Biggest Ring Around Saturn Just Got Supersized*. URL: https://www.space.com/29624-giant-saturn-ring-even-bigger.html.

Dikarev, V. (1999). "Dynamics of particles in Saturn's E ring: effects of charge variations and the plasma drag force". In: *Astronomy and Astrophysics, vol. 346*, pp. 1011–1019.

ESA (2018). *Cassini-Huygens Overview*. URL: https://www.esa.int/Our_Activities/Space_Science/Cassini-Huygens_overview.

Green, Daniel W. E. (2009). *S/2008 S 1*. URL: http://ciclops.org/view/5518/S2008_S_1?js=1.

Hamilton, D.P., M.F. Skrutskie, A.J. Verbiscer, and F.J. Masci (2015). "Small particles dominate Saturn's Phoebe ring to surprisingly large distances". In: *Nature, vol. 522*, pp. 185–187.

Hedman, M.M., J.A. Burns, M.R. Showalter, C.C. Porco, P.D. Nicholson, A.S. Bosh, M.S. Tiscareno, R.H. Brown, B.J. Buratti, K.H. Baines, and R. Clark (2006). "Saturn's dynamic D ring". In: *Icarus, vol. 188*, pp. 89–107.

Hedman, M.M., J.A. Burns, M.S. Tiscareno, C.C. Porco, G.H. Jones, E. Roussos, N. Krupp, C. Paranicas, and Sascha Kempf (2007). "The Source of Saturn's G Ring". In: *Science, vol. 317*, pp. 653–656.

Hedman, M.M., J.A. Burt, J.A. Burns, and M.S. Tiscareno (2010). "The shape and dynamics of a heliotropic dusty ringlet in the Cassini Division". In: *Icarus, vol. 210*, pp. 284–297.

Hedman, M.M., C.D. Murray, N.J. Cooper, M.S. Tiscareno, K. Beurle, M.W. Evans, and J.A. Burns (2009). "Three tenuous rings/arcs for three tiny moons". In: *Icarus, vol. 199*, pp. 378–386.

Horányi, M. (1996). "Charged Dust Dynamics in the Solar System". In: *Annual Review of Astronomy and Astrophysics, vol. 34*, pp. 383–418.

Horanyi, M., J.A. Burns, M.M. Hedman, G.H. Jones, and S. Kempf (2009). *Saturn from Cassini-Huygens*. Ed. by Michele K. Dougherty, Larry W. Esposito, and Stamatios M. Krimigis. Springer. Chap. 16, Diffuse Rings, pp. 511–536.

Howett, C.J.A., J.R. Spencer, J. Pearl, and M. Segura (2011). "High heat flow from Enceladus' south polar region measured using 10—600 cm^{-1} Cassini/CIRS data". In: *Journal of Geophysical Research, vol. 116*.

Hsu, H.-W., F. Postberg, S. Kempf, G. Moragas-Klostermeyer, M. Horanyi, M. Seiss, M. Burton, J. Schmidt, F. Spahn, J. Cuzzi, S. Ye, W. Kurth, D. Schirdewahn, J. O'Donoghue, N. Khawaja, and R. Srama (2018). "A dusty road connecting Saturn and its rings - preliminary results from Cassini Cosmic Dust Analyser during the Grand Finale Mission". In: 20th EGU General Assembly in Vienna, Austria.

Hsu, H.-W., F. Postberg, Y. Sekine, T. Shibuya, S. Kempf, M. Horányi, A. Juhász, N. Altobelli, K. Suzuki, Y. Masaki, T. Kuwatani, S. Tachibana, S. Sirono, G.

Moragas-Klostermeyer, and R. Srama (2015). "Ongoing hydrothermal activities within Enceladus". In: *Nature, vol. 519*, pp. 207–210.

Iess, L., B. Militzer, Y. Kaspi, P. Nicholson, D. Durante, P. Racioppa, A. Anabtawi, E. Galanti, W. Hubbard, M.J. Mariani, P. Tortora, S. Wahl, and M. Zannoni (2019). *Measurement and implications of Saturn's gravity field and ring mass*. URL: http://science.sciencemag.org/content/early/2019/01/16/science.aat2965.

Iess, L., D.J. Stevenson, M. Parisi, D. Hemingway, R.A. Jacobson, J.I. Lunine, F. Nimmo, J.W. Armstrong, S.W. Asmar, M. Ducci, and P. Tortora (2014). "The Gravity Field and Interior Structure of Enceladus". In: *Science, vol. 344*, pp. 78–80.

Ingersoll, A.P. and S.P. Ewald (2011). "Total particulate mass in Enceladus plumes and mass of Saturn's E ring inferred from Cassini ISS images". In: *Icarus, vol. 216*, pp. 492–506.

Juhász, A., M. Horányi, and G.E. Morfill (2007). "Signatures of Enceladus in Saturn's E ring". In: *Geophysical Research Letters, vol. 34, issue 9*.

Kempf, S., U. Beckmann, G. Moragas-Klostermeyer, F. Postberg, R. Srama, T. Economou, J. Schmidt, F. Spahn, and E. Grün (2008). "The E ring in the vicinity of Enceladus I. Spatial distribution and properties of the ring particles". In: *Icarus, vol. 193*, pp. 420–437.

Kempf, S., U. Beckmann, R. Srama, M. Horanyi, S. Auer, and E. Grün (2006). "The Electrostatic Potential of E Ring Particles". In: *Planetary and Space Science, vol. 54*, pp. 999–1006.

Kempf, S., R. Srama, and A. Graps (2012). *The Cosmic Dust Analyzer Data Handbook*. Version 0.1.

Madeira, G., R. Sfair, D.C. Mourao, and S.M. Giuliatti-Winter (2018). "Production and fate of the G ring arc particles due to Aegaeon". In: *Monthly Notices of the Royal Astronomical Society, vol. 475*, pp. 5474–5479.

Mankovich, C., M.S. Marley, J.J. Fortney, and N. Movshovitz (2019). "Cassini Ring Seismology as a Probe of Saturn's Interior I: Rigid Rotation". In: *The Astrophysical Journal, vol. 871*.

NASA (2017a). *Iapetus, In depth*. URL: https://solarsystem.nasa.gov/moons/saturn-moons/iapetus/in-depth/.

— (2017b). *NASA Missions Provide New Insights into 'Ocean Worlds' in Our Solar System*. URL: https://www.nasa.gov/press-release/nasa-missions-provide-new-insights-into-ocean-worlds-in-our-solar-system.

— (2017c). *Pallene, In depth*. URL: https://solarsystem.nasa.gov/moons/saturn-moons/pallene/in-depth/.

— (2018). *Cassini Legacy 1997-2017*. URL: https://solarsystem.nasa.gov/missions/cassini/overview/.

Oergerle, William (2004). *Walter Alexander Feibelman (1925 - 2004)*. URL: https://aas.org/obituaries/walter-alexander-feibelman-1925-2004.

Porco, C.C., P. Helfenstein, P.C. Thomas, A.P. Ingersoll, J. Wisdom, R. West, G. Neukum, T. Denk, R. Wagner, T. Roatsch, S. Kieffer, E. Turtle, A. McEwen, T.V. Johnson, J. Rathbun, J. Veverka, D. Wilson, J. Perry, J. Spitale, A. Brahic, J.A. Burns, A.D. Del Genio, L. Dones, C.D. Murray, and S. Squyres (2006).

"Cassini Observes the Active South Pole of Enceladus". In: *Science*, *vol. 311*, pp. 1393–1401.

Postberg, F., S. Kempf, J.K. Hillier, R. Srama, S.F. Green, N. McBride, and E. Grün (2008). "The E-ring in the vicinity of Enceladus II. Probing the moon's interior — The composition of E-ring particles". In: *Icarus*, *vol. 193*, pp. 438–454.

Postberg, F., S. Kempf, J. Schmidt, N. Brilliantov, A. Beinsen, B. Abel, U. Buck, and R. Srama (2009). "Sodium salts in E-ring ice grains from an ocean below the surface of Enceladus". In: *Nature*, *vol. 459*, pp. 1098–1101.

Postberg, F., N. Khawaja, B. Abel, G. Choblet, C.R. Glein, M.S. Gudipati, B.L. Henderson, H.-W. Hsu, S. Kempf, F. Klenner, G. Moragas-Klostermeyer, B. Magee, L. Nölle, M. Perry, R. Reviol, J. Schmidt, R. Srama, F. Stolz, G. Tobie, M. Trieloff, and J.H. Waite (2018). "Macromolecular organic compounds from the depths of Enceladus". In: *Nature*, *vol. 558*, pp. 564–568.

Postberg, F., J. Schmidt, J. Hillier, S. Kempf, and R. Srama (2011). "A salt-water reservoir as the source of a compositionally stratified plume on Enceladus - Supplementary information". In: *Nature*, *vol. 474*, pp. 620–622.

Schmidt, J., N. Brilliantov, F. Spahn, and S. Kempf (2008). "Slow dust in Enceladus' plume from condensation and wall collisions in tiger stripe fractures". In: *Nature*, *vol. 451*, pp. 685–688.

Schmidt, J., R. Srama, and S. Kempf (2017). "Personal communications".

Seiss, M., R. Srama, S. Kempf, K.L. Sun, M. Seiler, M. Sachse, G. Moragas-Klostermeyer, and F. Spahn (2014). "Pallene dust torus". In: American Geophysical Union, Fall Meeting 2014.

Spahn, F., J. Schmidt, N. Albers, M. Hörning, M. Makuch, M. Seiß, S. Kempf, R. Srama, V. Dikarev, S. Helfert, G. Moragas-Klostermeyer, A.V. Krivov, M. Sremčević, A.J. Tuzzolino, T. Economou, and E. Grün (2006). "Cassini Dust Measurements at Enceladus and Implications for the Origin of the E Ring". In: *Science*, *vol. 311*, pp. 1416–1418.

Spencer, J.R. and T. Denk (2010). "Formation of Iapetus' Extreme Albedo Dichotomy by Exogenically Triggered Thermal Ice Migration". In: *Science*, *vol. 327*, pp. 432–435.

Spencer, J.R., J.C. Pearl, M. Segura, F.M. Flasar, A. Mamoutkine, P. Romani, B.J. Buratti, A.R. Hendrix, L.J. Spilker, and R.M.C. Lopes (2006). "Cassini Encounters Enceladus: Background and the Discovery of a South Polar Hot Spot". In: *Science*, *vol. 311*, pp. 1401–1405.

Srama, R., T.J. Ahrens, N. Altobelli, S. Auer, J.G. Bradley, M. Burton, V.V. Dikarev, T. Economou, H. Fechtig, M. Görlich, M. Grande, A. Graps, E. Grün, O. Havnes, S. Helfert, M. Horanyi, E. Igenbergs, E.K. Jessberger, T.V. Johnson, S. Kempf, A.V. Krivov, H. Krüger, A. Mocker-Ahlreep, G. Moragas-Klostermeyer, P. Lamy, M. Landgraf, D. Linkert, G. Linkert, F. Lura, J.A.M. McDonnell, D. Möhlmann, G.E. Morfill, M. Müller, M. Roy, G. Schäfer, G. Schlotzhauer, G.H. Schwehm, F. Spahn, M. Stübig, J. Svestka, V. Tschernjawski, A.J. Tuzzolino, R. Wäsch, and H.A. Zook (2004). "The Cassini Cosmic Dust Analyzer". In: *Space Science Reviews*, *vol. 114*, pp. 465–518.

Sun, K.-L., J. Schmidt, and F. Spahn (2015). "Particle dynamics in the central ringlet of Saturn's Encke gap". In: *eprint arXiv:1510.07730*.

Thomas, P.C., R. Tajeddine, M.S. Tiscareno, J.A. Burns, J. Joseph, T.J. Loredo, P. Helfenstein, and C. Porco (2016). "Enceladus's measured physical libration requires a global subsurface ocean". In: *Icarus*, *vol. 264*, pp. 37–47.

University of Chicago News (2008). *Anthony Tuzzolino, Space Physicist, 1931-2008*. URL: https://news.uchicago.edu/story/anthony-tuzzolino-space-physicist-1931-2008.

Verbiscer, A.J., M.F. Skrutskie, and D.P. Hamilton (2009). "Saturn's largest ring". In: *Nature*, *vol. 461*, pp. 1098–1100.

Waite, J.H., C.R. Glein, R.S. Perryman, B.D. Teolis, B.A. Magee, G. Miller, J. Grimes, M.E. Perry, K.E. Miller, A. Bouquet, J.I. Lunine, T. Brockwell, and S.J. Bolton (2017). "Cassini finds molecular hydrogen in the Enceladus plume: Evidence for hydrothermal processes". In: *Science*, *vol. 356*, pp. 155–159.